Distortion Effect in Geometry of Prismatic Thin Wall Parts of AA2014-T651 During Machining

N.Vinaya Kumar
Research scholar in Mechanical Engineering
JNTU, Hyderabad, India
vnkmrnalla@gmail.com

Dr. M. Indira Rani
Professor in Mechanical Engineering
JNTUH college of Engineering, Hyderabad, India
marpuindira@gmail.com

Abstract

Thin wall parts distort due to redistribution of unbalanced residual stresses after material removal. This distortion is due to generation of bending moment on parts during material removal. Prismatic slender AA2014 models were analyzed by transient thermal analysis and structural analysis with finite element software for geometric distortion against nominal dimensions by incorporating solution treatment properties and then initial stresses and strains into the analysis model for achieving T6 condition. Subsequently, the model was prepared by reducing it to 90% of pre-stresses to simulate stretched model conditions to map with T651 condition. Subsequently, total deformation was analyzed by material removal using birth and death technique for T651 condition models by incorporation of proportional stresses and strains, by applying correction factor, were evaluated in physical experiment by slitting method strain gauge method. Simulation experiments were carried out with corrected model to evaluate total deformation by layer removal. Deformation results were used for statistical analysis to study the effect of geometrical parameters on distortion trend. It is found that length of the part has significant effect on distortion. This analysis is useful for designing of prismatic slender parts for considering geometry effect on distortion of AA2014 T651, which can be a guide during design for incorporating reinforcements to minimize distortion after material removal.

Keywords
Transient Thermal Analysis, Structural Analysis, AA2014-T651, Residual Stresses, Birth and Death technique

1. Introduction

Thin wall geometry parts made of AA2014-T651 are used in structural applications of avionic systems due to its unique characteristics like light weight and electric conductivity, its raw material mechanical properties of AA2014 are improved by solution treatment, but residual stresses are increased due to sudden quenching, which are then processed by stretched stress relieving and artificial ageing. Chetalin et al.(2011)stated as the interactions between existing component flaws, in-service loading conditions, and internal residual stresses typically determine how long a structural part will last when used in aerospace. The residual stresses (RS) may be advantageous or detrimental for the component depending on their nature, distribution, or magnitude; neither outcome is assured. Depending on the specific situation, the residual stresses may be insignificant or important. The residual stresses are always increased by each of the several manufacturing procedures used to create components, leading to a final distribution that affects the mechanical characteristics and results in dimensional and geometrical deviations for the part features. Chetalin et al.(2011) investigated distortions caused by residual stresses in work parts using AA7050-T7451 thin wall parts. They concluded that the initial residual stresses in raw materials have an effect on the deformation of the final part. Machining-induced residual stresses have a particularly large impact on part distortion in thin monolithic aerospace components. All of these factors influence the final distribution of residual stresses, which influences component distortion. According to Gao et al. (2017) the distortion caused by the initial RS in the machining process can cause a number of issues, including increased production time and component costs. These distortions also reduce component service life and may result in the parts being scrapped entirely. As a result, RS measurement

accuracy is critical to avoiding adverse effects on aircraft performance. Schulze et al. (2013) conducted experiments and finite element simulations on AA7075 -T6to investigate the relationship between residual stress and deformation and concluded that distortion is dependent on initial residual stresses and induced stresses are generated by manufacturing processes such as heat treatment, forming, or machining. Robinson et al. (2011) analyzed FEM model of AA7449 by considering average heat transfer coefficient of 12,000 Wm−2 K−1, and maximum compressive stress was observed as -184 MPa and maximum tensile stress was observed as 213 MPa by neutron diffraction method and also concluded as redistribution of stresses is the main cause for deformation.

Sridhar and Ramesh Babu (2018) conducted an experimental and numerical study on AA2014-T651 to investigate the effect of tool helix angle, direction, and number of flutes on the distortion of thin-walled parts. It was discovered that tool geometry parameters and a lower number of flutes had a significant impact on wall distortion. Huang et al., (2015) used FEM and experiments AA7050-T7451 to investigate the machining deformation of a beam part caused by Machining induced residual stress (MIRS), Initial residual stress (IRS), and the coupling of these two factors. According to the findings, IRS dominated machining deformation and accounted for 90% of total deformation, while MIRS contributed about 10%.Izamshah et al. [2013] investigated the impact of end mill helix angle variation on precision when cutting thin-rib aerospace components of AA7056. When compared to a tool with a smaller diameter, it was found that a wider helix angle created the least chatter and therefore the least surface inaccuracy due to cutting forces, stress distribution, chip deformation, cutting edge stiffness, and tool rigidity can all be significantly impacted by rake angle. Jiang et al. (2013) concluded by experimentation on AA7050-T7451as optimum cutter diameter during machining, in their experiment, found that increasing in diameter of cutter, deformation still reduces due to residual stress transforms to more uniform after conducting simulation and machining experiments and observed that maximum deformation value is lowered by 63.8% with increase in tool diameter from 6 mm to 12 mm. Liu et al. (2015) developed a FE model to calculate the deformation of an aluminum alloy AA 7075 part while taking the IRS of the blank into account and identified these stresses are redistributed during machining after material removal for more than half of the blank. Taguchi approach experiments by Sridhar and Ramesh Babu (2013) on the material AA2014-T651 revealed that the depth of cut and width of cut have a substantial impact on machining distortion. Masoudi et al. (2015) investigated the relationship between machining residual stress and AA7075-T6thin-walled part machining distortion. The results demonstrated that increasing machining residual stress causes an increase in work piece distortion, and it was also concluded that polycrystalline diamond (PCD) tools can reduce distortion. On Aluminum 7050-T7451, Tang et al. (2013) developed a machining prediction model using FEM and noted that the primary causes of machining deformation include the initial residual stress, machining induced residual stress, clamping force, cutting force, as well as cutting heat. Wei et al. (2007) used experiments and finite element analysis (FEA) to estimate deflection on AA7050-T7451, and the results showed that longitudinal residual stress is greater than lateral residual stress if the specimen's length is greater than its breadth.

Koc et al. (2006) Quenching is a technique used in the heat treatment of AA7050 forging block to achieve the desired mechanical properties. This process is regarded as the most important factor in the formation of residual stress in materials, which were reduced up to 90% by stretching up to 2%. Yang et al. (2013) used a cold stretching technique (1.5% stretching at a speed of 0.5 mm/s), successfully reducing the quenching residual stress of an A357 aluminum alloy cylindrical bar by 81.5-94.9% through experimentation at various temperatures. They also came to the conclusion that higher quenching temperatures for the blanks result in lower maximum tensile and compressive stresses.

Even though initial residual stresses are reduced by stretching, balance stresses are effect on the thin wall parts geometry thus distort the thin wall parts. Hence, aircraft components' weight is to be reduced and material performance is to be improved by prediction of distortion and providing suitable supports to minimize the distortion. Researchers have worked a lot on distortion due to initial stresses effect and machining induced stresses, but prediction of deformation against internal residual stresses is limited for AA2014-T651 by consideration of quench delay time. In this paper prediction of deformation of AA2014-T651 is done by considering quenching stresses and geometry control factors and also its effects on distortion.

1.1. Objectives

The aim of this work is to predict deformation of AA2014-T651 on prismatic slender thin wall parts using FEM model by transient thermal analysis, structural analysis and experimentation to evaluate residual stress by slitting method and analyzing of geometry parameters using statistical tools.

2. Simulation and experimentation

Residual stresses are developed during solution treatment of Heat treatable aluminum alloy plates or sheets, these stresses are balanced by internal rigidity of the material. These stresses are unbalanced during material removal and redistributed which act as bending stresses on the final geometry. The blanks are stretched to relieve internal stresses. These blanks are sized for ready to use, which are generally 1000 x 1000 mm sizes and more sizes are also being produced. However, residual stresses are not uniform throughout the blank, which vary with respective to the thermal gradient during solution treatment process. Hence, Controlling of distortion during machining of these blanks is difficult.

Residual stresses and distortion were analyzed in the different size models as per Taguchi Orthogonal table, which were simulated to get properties of AA2014-T651 by transient thermal analysis and structural analysis of solution treatment by considering each blank as solution treated, further stretch relieved for reduction of residual stresses without inducing internal stresses in order to analyze the geometry effects. The geometry models used for simulation experiment are shown in Figure 1(a) and Figure 1 (b) for blank and after material removal.

Distortion occurs due to the unbalanced residual stresses acting on the final geometry of the parts during machining. Deformation is function of internal stresses and strains for solution treated (quenching) of raw materials and which depend upon the raw material and its blank size.

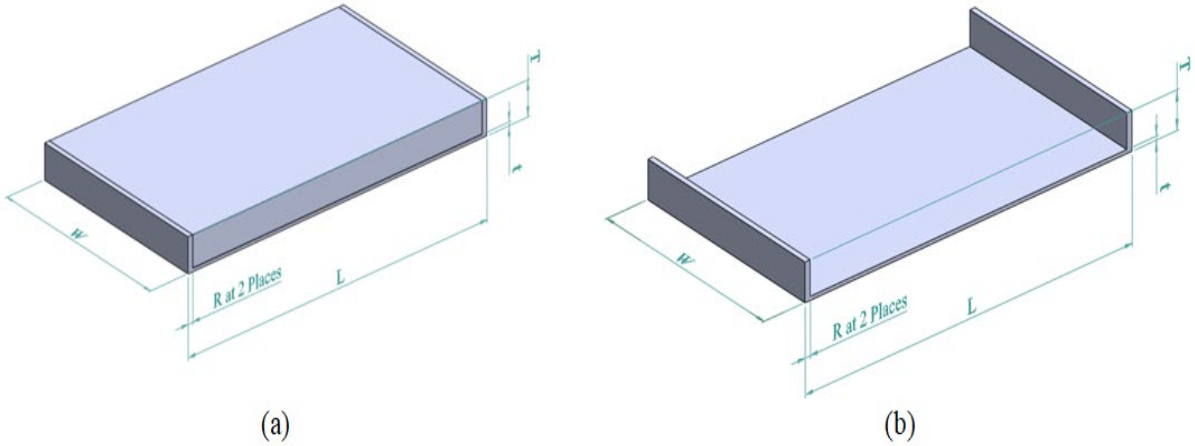

Figure 1. Model with dimensions: (a) Blank and (b) After material removal
All dimensions are in mm.

Deformation (δ), due to unbalanced forces of residual stresses acting on elementary areas is shown in Figure 2. The deformation function is shown in Eq. 1 and Eq. 2.

δ = f (internal stresses, internal strains, geometrical dimensions) - - - - - - - Eq.1

$\delta = f(\sigma_x, \sigma_y, \sigma_z, \tau_{xy}, \tau_{yz}, \tau_{xz}, \varepsilon_x, \varepsilon_y, \varepsilon_z, \gamma_{xy}, \gamma_{yz}, \gamma_{zx}, \varepsilon_{tx}, \varepsilon_{ty}, \varepsilon_{tz}, \varepsilon_p, dx, dy, dz)$ - - - - - - Eq.2

Here,

- Normal stresses in x, y and z directions as σ_x, σ_y and σ_z respectively and shear stresses in xy, yz and xz balanced on elemental free body.
- Normal elastic strains in x, y and z directions as ε_x, ε_y and ε_z respectively.
- Shear strains in xy, yz and xz plane as γ_{xy}, γ_{yz} and γ_{zx} respectively.
- Thermal strains in x, y and z directions as ε_{tx}, ε_{ty} and ε_{tz} respectively.
- Plastic strains (ε_p)

Unbalanced force (F) acting on elementary area is given in Eq. 3

$F = \int \sigma . dA$ - - - - - - -- Eq.3

Bending moment (M) on elementary area, if considered as plane beam, is given in Eq. 4and Eq. 5

$M = \int \sigma.y.\, dA$ - - - - - - - Eq.4
$M = \sigma.z$ - - - - - - - Eq.5
Here, σ = Unbalanced residual stress in the model.
y = Distance between unbalanced force position to center of elementary area.
z = Section modulus of the model.

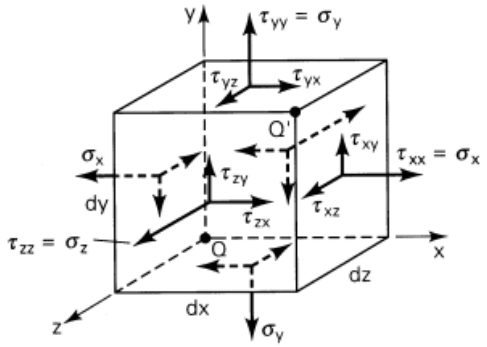

Figure 2. Stresses acting on elemental free body

Distortion due to bending moment depends upon internal stresses and section modulus. Its effect due to unbalanced residual stress in the model and also rigidity of the material depends upon the section modulus and centroid of the part. So each dimension of the model is affected by the distortion and deformation due to unbalanced residual forces after machining. Here, residual stresses are not controllable and section modulus can be controlled at design stage for machined parts to control the distortion.

Models were created with dimensions mentioned in **L_{27}** Taguchi orthogonal table shown at Table 1 against length (L), width (W), Rib thickness (R), final thickness (t) and total thickness (T). These dimensions were considered as control parameters for Taguchi orthogonal table given at Table 1 for simulating thermal and structural analysis. Figure 1(a) and Figure 1(b) give details of blank and thin walled model after material removal respectively. Response factors were considered as minimum principal stress and deformation for transient thermal and structural analysis.

Practically, thin wall parts are distorted due to effect of stresses and strains during solution treatment (quenching), calculation of these stresses, strains and its deformation is difficult analytically. Hence, FEM modeling was used to simulate the deformation on thin wall prismatic parts using above mentioned inputs and further which were analyzed using MINITAB statistical tools.

2.1 Material and analytical parameters

Material AA2014 properties were incorporated into ANSYS engineering data further to create T6 and T651 properties assuming material as isentropic and flexible model.

In Transient thermal analysis to incorporate T6 properties the following parameters were considered:
- Solution treatment temperature as 502°C (ASM Handbook Volume 4).
- Convection film coefficient as 28500 W/m^2.°C (2.85 W/cm^2.K) at 60°C and 35500 W/m^2.°C (3.55W/cm^2.K) at 26°C (ASM Handbook Volume 4) in order to simulate quenching delay within 10 seconds.
- Ambient temperature as 26°C.

2.2 FEM modeling

Geometry model was created in two layers one for blank and other for final machined part. These two layers were bonded as removable material and final part FEM modeling was carried out in ANSYS 19.0 by simulating Transient thermal analysis and structural analysis.
Transient thermal analysis was simulated by inducing multi-linear isentropic hardening material properties for modeling of quenching effect in order to induce solution treatment properties in AA2014 model and these solution results were imported into structural analysis and model was simulated by fixing at 3 corner points and solved to get

principal stresses and strains in models of AA2014-T6. Subsequently, the model was prepared by reducing it to 90% of pre-stresses to simulate stretched model conditions to map with T651 condition. Further, total deformation was analyzed by material removing using birth and death technique in ANSYS for T651 models.

Analysis procedure details are as following:

a. Material details inclusion in engineering data.
b. Creation of Geometrical models in composite of two layers as mentioned in Figure 1 (a) and in orthogonal Table 1.
c. Transient thermal analysis.
d. Thermal load import to structural analysis I.
e. Structural analysis I.
f. Created results in order to export initial stresses and strains as σ_x, σ_y,σ_z, τ_{xy}, τ_{yz}, τ_{xz} , ε_x, ε_y,ε_z, γ_{xy}, γ_{yz}, γ_{zx}, ε_{tx}, ε_{ty}, ε_{tz} and plastic strains (ε_p) were considered as a null.
g. Structural analysis II:
   Imported previous results by reducing intensity to 90% in order to get T651 properties.
h. Machining model:
   Removed machining layer as per orthogonal table and experimental model in order to simulate machining.
i. Final result evaluated as deformation.

Flow chart of FEM analysis procedure is shown in Figure 3.

Table 1. Taguchi orthogonal table with control factors, results and signal to noise ratios of Experiments for AA2014- T651

	Control factors					Results		Signal to noise ratios	
Sl. No	Length (L in mm)	Width (W in mm)	Ribs thickness (R in mm)	Final thickness (t in mm)	Total thickness (T in mm)	Deformation (δ in mm)	Minimum principal stress (-σ in MPa)	SNRA for deformation	SNRA for Minimum principal stress
1	42	24	1	1	6	0.253	108.85	11.93759	-40.7366
2	42	24	1	1	8	0.192	108.85	14.33398	-40.7366
3	42	24	1	1	10	0.198	108.26	14.0667	-40.6894
4	42	48	2	2	6	0.327	122.47	9.709045	-41.7606
5	42	48	2	2	8	0.285	88.215	10.9031	-38.9108
6	42	48	2	2	10	0.268	91.4	11.4373	-39.2189
7	42	72	3	3	6	0.298	82.968	10.51567	-38.3782
8	42	72	3	3	8	0.31	71.977	10.17277	-37.1439
9	42	72	3	3	10	0.287	86.29	10.84236	-38.7192
10	84	24	2	3	6	0.333	99.626	9.551115	-39.9675
11	84	24	2	3	8	0.249	99.626	12.07601	-39.9675
12	84	24	2	3	10	0.349	97.564	9.143491	-39.7858
13	84	48	3	1	6	0.537	75.579	5.400514	-37.568
14	84	48	3	1	8	0.545	89.505	5.27207	-39.0369
15	84	48	3	1	10	0.538	73.019	5.384354	-37.2687
16	84	72	1	2	6	0.5	128.2	6.0206	-42.1578
17	84	72	1	2	8	0.556	163.35	5.098504	-44.2624
18	84	72	1	2	10	0.617	204.23	4.194297	-46.2024
19	126	24	3	2	6	0.818	85.638	1.744934	-38.6533
20	126	24	3	2	8	0.881	110.9	1.100482	-40.8986
21	126	24	3	2	10	0.904	77.559	0.876631	-37.7926
22	126	48	1	3	6	0.543	163.42	5.304003	-44.2661
23	126	48	1	3	8	0.456	150.18	6.820703	-43.5322
24	126	48	1	3	10	0.503	199.48	5.96864	-45.998
25	126	72	2	1	6	0.656	122.09	3.661923	-41.7336
26	126	72	2	1	8	0.662	284.92	3.58284	-49.0945
27	126	72	2	1	10	0.645	197.6	3.808806	-45.9157

Sample FEM model results for experiment number 27 of Transient thermal analysis, Structural analysis-I and Structural analysis-II were shown in Figure 4 (a), Figure 4 (b) and Figure 5 respectively.FEM model final results were evaluated as total deformation of machined block and minimum principal stress of un- machined block and also signal to noise ratio of results are shown against experiment numbers in Table 1.Residual stress is not same all over the surface of wrought plates, which is varied with respective to the thermal gradient. So, stress is different in a blank in the wrought plates to analyze this effect Correction factor, it is shown in Eq. 6, was introduced to incorporate equivalent residual stresses and strains in the FEM model.

$$\text{Correction factor}=\frac{|\text{Physical stress maximum value}|}{|\text{Minimum principal stress value}|} \quad \text{---------- Eq.6}$$

Here, Minimum principal stress value is in FEM model at structural analysis-I and its correction factor was considered as 0.1 for AA2014-T651 at maximum residual stress condition to import residual stresses as initial stresses and strains at structural analysis-II. Physical stress maximum value, evaluated in the sample, was used to predict the deformation in physical parts by applying correction factor in the structural analysis-II.

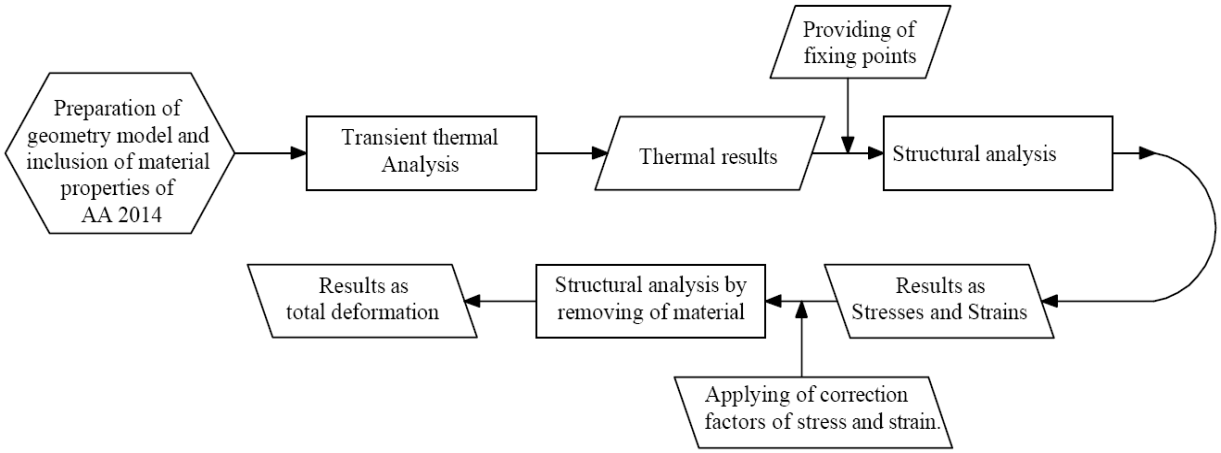

Figure 3. Flow chart for FEM modeling

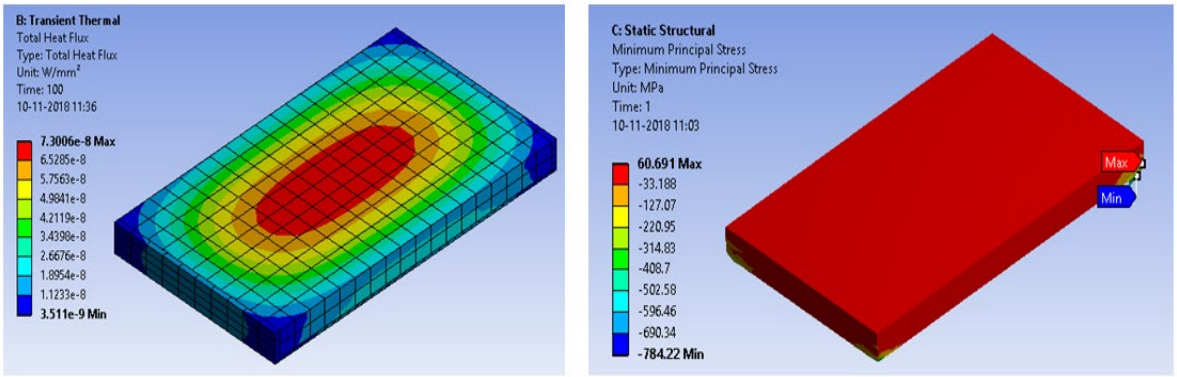

(a) (b)

Figure 4. Experiment no.27 FEA analysis: (a) Transient thermal analysis and (b) Structural analysis-I
All input and output values are in SI units.

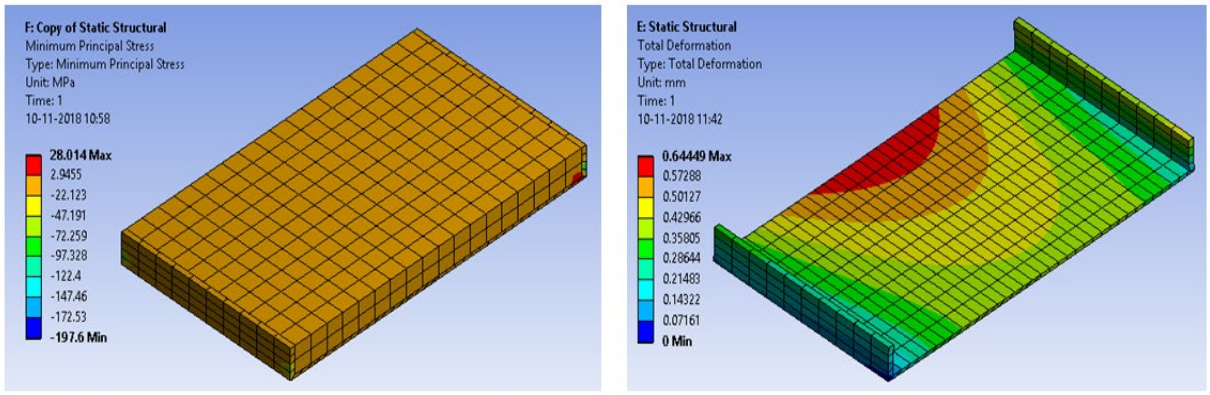

Figure 5. Structural analysis for exp.no.27 at correction factor 0.1: (a) Minimum principal stress and (b)Deformation
All input and output values are in SI units.

2.3 Evaluation of residual stress on physical experiment

A physical sample 6 mm x 25 mm x 25 mm of Aluminum alloy 2014-T651 with same heat number of validation sample was taken for evaluating residual stresses by slitting residual strain gauge method (Cheng et al. 2007). Milling was carried out on both sides of sample and maintained thickness 5.0 mm for removing of Alclad material. A strain gauge NIE NIA 350±0.3 Ohm, G.F.-2.11 was bonded with Loctite 406 on the sample. Strain gauge pads were soldered by insulated copper wires for measurements as shown in Figure 6. Sample was mounted in vice of Three axis CNC vertical milling machine and slitting operation was carried out for 2.0 mm width slot using Ø2.0 mm solid carbide slot drill with dry machining and cutting parameters as 0.25 mm depth of cut, 3000 RPM and feed 300 mm/minute. Resistance of strain gauge was measured using KEYSIGHT 34461A $6\frac{1}{2}$ Digital Multimeter for every 0.5 mm depth of cut and final depth as 4.0 mm on opposite side of strain gauge at center axis of strain gauge. Residual stresses were evaluated against its strain gauge resistance values using Eq. 7 and Eq.8, stress values are shown in Figure 7. Further, a physical component was made on wire-cut EDM machine to avoid machining residual stresses and result deformation was measured.

Strain (ε) = [Change in resistance/Initial resistance]/Gauge factor

$$\varepsilon = \left[\frac{\Delta R}{R}\right] / GF \quad \text{- - - - - - - - - - - Eq.7}$$

Residual stress = Young Modulus x strain

$$\sigma = E.\,\varepsilon. \quad \text{- - - - - - - - - - - - -Eq.8}$$

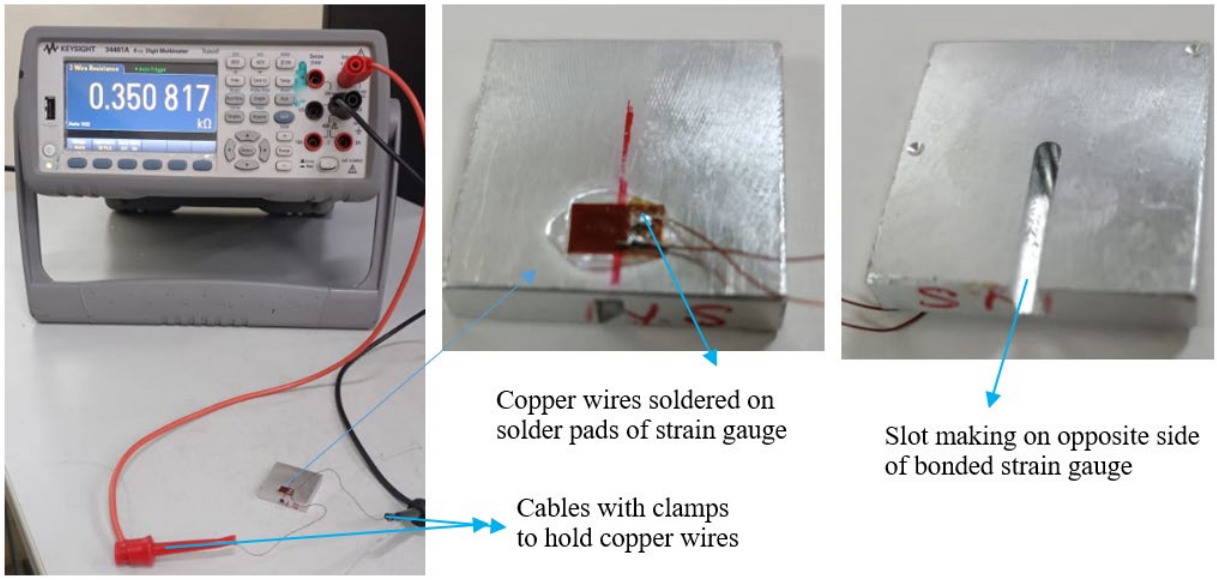

Figure 6. Resistance of strain gauge measuring on KEYSIGHT 34461A $6\frac{1}{2}$ Digital Multimeter on slotted sample.

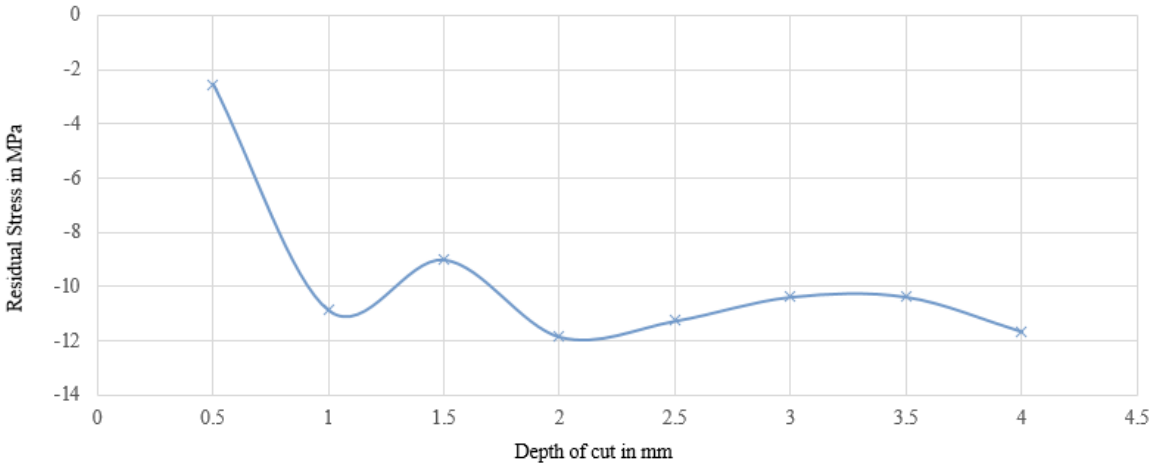

Figure 7.Graph for Depth of cut vs Residual stress in 6 mm blank of AA2014-T651.

3. Results and Discussion

Experimental results, minimum principal stress and deformation, were analyzed against geometry control factors at 95% confidence level using Minitab statistical software.

3.1. Analyzing for un-machined block

Residual stresses were induced in the wrought aluminum plates due to residual quenching stresses during solution treatment of AA2014 raw material. Maximum compressive stress is a minimum principal stress (σ) in the FEM model, which was considered as a result of transient thermal and structural analysis in the first stage, here geometry parameters length (L), width (W) and total thickness (T) were considered in the discussion due to un-machined block and remaining geometry parameters ribs thickness 'R' and final thickness (t) were considered as imaginary at first stage. Signal to noise ratio of minimum principal stress was considered as 'smaller is better' against geometry control factors due to lower residual stresses minimize the deformation for un-machined AA2014-T651, which is

shown in Figure 8 for Main effects plot for SN ratios for minimum principal stress against geometry control factors for Un-machined AA2014-T651.

Effect of geometry control factors on minimum principal stress discussed with reference to Figure 8:

- Residual stress decreases by reducing length and width of the thin wall parts due to thermal gradient variation is reduced if the block size decreases.
- Minimum principal stresses reduce, by increasing ribs thickness and final thickness dimensions in the machined thin wall parts, as robustness increases. These geometry control factors are imaginary due to which are final dimensions in the machined thin wall parts.
- Signal to noise ratio for thickness is nonlinear due to minimum principal stresses depend upon thermal gradient along the thickness. However its SN ratio variation is very less.

Effect of geometry control factors on minimum principal stress discussed with reference to Analysis of variance (ANOVA) Table 2:

- Minimum principal stress mainly depends upon length and width combination of raw material and its contribution is 31.75%, alone length contribution is 23.45% and then followed by width contribution is 16.67% due to dissipation of heat during quenching depends on the surface area.
- Remaining factors and combination of factors such as T, L*T, W*T and L*W*T are not much contributed on minimum principal stress.

Regression equation fit regression model is used for minimum principal stress (σ) equation at R-sq. 95.28% and R-sq. (prediction) 88.64%, which is mentioned at Eq. 9.

$$\sigma = 1.519\ L + 2.01\ W + 18.31\ T - 0.0342\ L*W - 0.301\ L*T - 0.469\ W*T + 0.00842\ L*W*T \quad \text{- - - - - - - Eq.9}$$

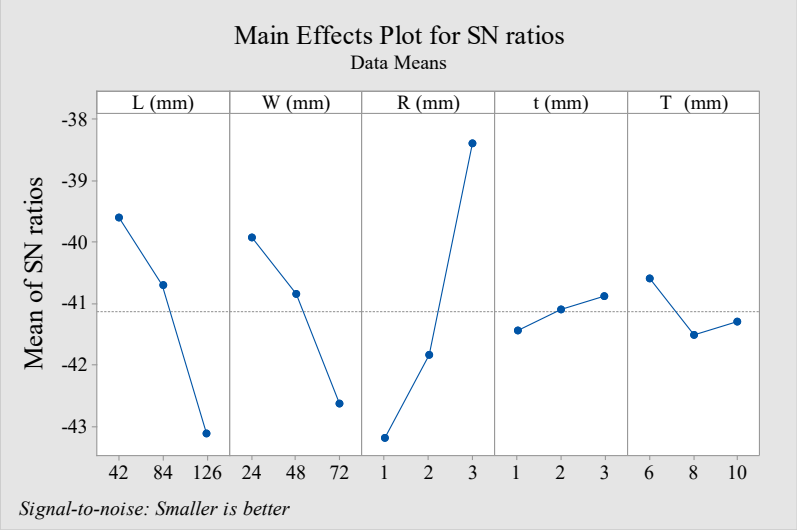

Figure 8. Main effects plot for SN ratios for minimum principal stress against geometry control factors for Un-machined AA2014-T651.

Table 2. ANOVA for Minimum principal stress against control factors for Un-machined AA2014-T651.

Factors	DF	Adj SS (SS_A)	Adj MS (V_A)	Percentage contribution = (SS_A-V_e*V_A) x 100 /SS_T
L	2	15906	7952.9	23.45
W	2	11312	5655.8	16.67
T	2	2016	1008.1	2.97

L * W	4	21534	5383.5	**31.75**
L * T	4	4375	1093.7	6.45
W * T	4	5146	1286.4	7.58
L * W * T	8	7535	941.9	11.1
Error	0	0	$V_e = 0$	
Total	26	$SS_T = 7823$		100

3.2 Analyzing for machined block

Maximum deformation values were considered as a final result of structural analysis in the FEM model to analyze the effect in the machined block. Distortion occurred in slender prismatic thin wall parts due to redistribution of unbalanced residual stresses/internal stresses during machining.

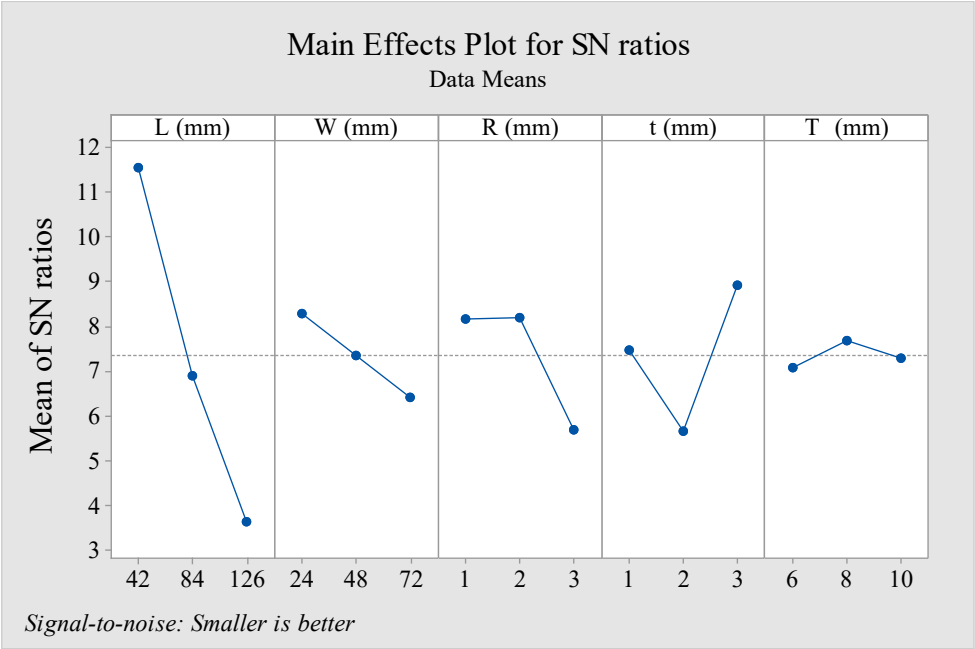

Figure 9. Main effects plot for SN ratios for Deformation against geometry control factors for machined AA2014-T651.

Thin wall parts robustness depends upon its geometry parameters due to bending moment during redistribution of residual stresses. Signal to noise ratio is considered as 'smaller is better' for deformation against geometry control factors for machined AA2014-T651,which is shown in Figure 9 for Main effects plot for SN ratios for deformation against geometry control factors for machined AA2014-T651.

Effect of geometry control factors on deformation discussed with reference to Figure 9:

- Deformation reduces if the length and width decreases due to thermal gradient residual stresses reduce as mentioned in Para 3.1.
- Signal to noise ratio for ribs thickness, final thickness and total thickness are shown non uniform results due to which mainly depend on minimum principal/initial residual stresses.

Effect of geometry control factors on deformation discussed with reference to Analysis of variance (ANOVA) Table 3:

- Deformation mainly depends upon length and its contribution is 67.45%≈67.5% due to existed geometry in the model, ribs are not provided along the width dimension. Hence, ribs are important to increase robustness in thin wall parts and to resist bending during redistribution of stresses.
- Final thickness and ribs thickness contribution is 16.9% and 11.8% respectively, which are followed by length, in deformation of thin wall parts due to redistribution of stresses during material removal. Remaining geometry factors, width and final thickness, are not much influence on the deformation.

Table 3. ANOVA for deformation against geometry control factors for machined AA2014-T651

Factors	DF	Adj SS (SS_A)	Adj MS (V_A)	Percentage contribution = (SS_A-V_e*V_A) x 100 /SS_T
L (mm)	2	0.74	0.37008	**67.45**
W (mm)	2	0.01	0.00807	1.47
R (mm)	2	0.12	0.06478	11.8
t (mm)	2	0.18	0.09283	16.9
T (mm)	2	0.0018	0.0009	0.164
Error	16	0.02	V_e =0.00144	2.11
Total	26	SS_T= 1.09	0.042	99.99

Deformation is not only dependent on geometrical parameters but also on internal stresses for this minimum principal stress was added as response. Its regression equation fit regression model is used for deformation (δ) equation at R-sq.99.43%and R-sq. (prediction) 97.86%, which is mentioned at Eq. 10.

$$\delta = 0.000648\ \sigma + 0.00917\ L + 0.01039\ W - 0.0283\ R - 0.1671\ t - 0.0700\ T - 0.000117\ L*W + 0.000842\ L*T + 0.001242\ W*T - 0.000015\ L*W*T \quad \text{Eq.10}$$

3.3 Validation experiment

Validation experiments were carried out using FEM model along with regression model and machining experiments. Analysis and experimentation results of deformation were confirmed using FEM model and regression model equations for length 126.0 mm, width 72.0 mm, ribs thickness 0.6 mm, final thickness 1.0 mm and total thickness 6 mm, which are shown in Figure 10 (a) and Figure 10 (b), and its results are shown in Table 4. Physical component was made on wire-cut EDM machine to avoid machining residual stresses and result deformation was measured and shown in Table 4 and Figure 11.

Table 4. Deformation values in Validation experiment

	Deformation		
Evaluated stress On sample	FEM model	Regression equation	Physical component
Minimum principal stress 11.8 MPa in slitting method	0.59 mm with correction factor 0.02783	0.58 mm	0.145+0.3171= 0.4621 mm

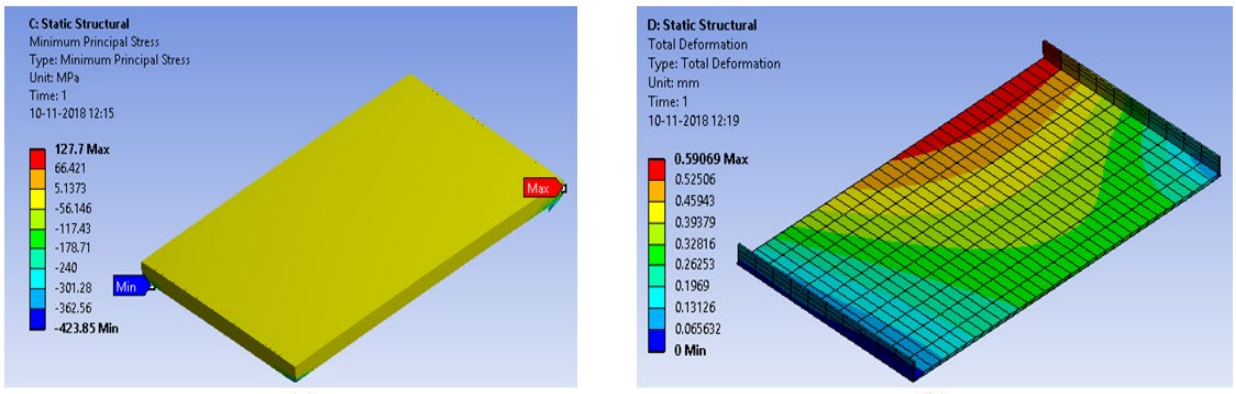

(a) (b)

Figure 10. Validation experiment in FEA analysis: (a) Minimum principal stress and (b) Deformation.

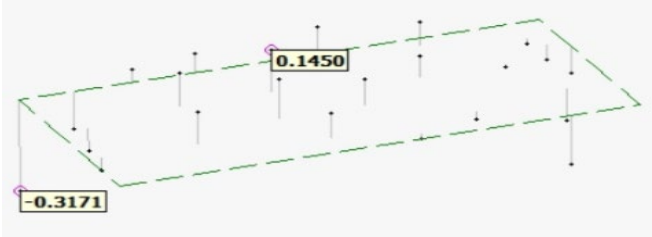

Figure 11. Deformation measuring on Micro-Vu vertex-311HC
for validation of physical component

Physical component deformation is 79.8% ≈ 80% of predicted deformation in FEM model and Regression equation. Hence deformation can be predicted using proposed FEM model.

4. Conclusions

The following conclusions can be drawn by the analysis of distortion on slender prismatic thin wall part using FEM model and statistical models.

- Residual stresses in AA2014-T651 properties were achieved by using FEM model and simulation in order to estimate the deformation.
- Minimum principal stress mainly depends upon length and width combination of raw material and its contribution is 31.75%.
- Deformation can be estimated using regression model equation in AA2014-T651 by considering geometrical parameters and residual stress.
- Deformation can be predicted using correction factor by comparing physical components using minimum principal stresses through FEM model.
- Deformation mainly depends on internal stresses as compared with geometrical parameters.
- This Deformation model can be used as a guide for providing ribs at appropriate places to avoid distortion during design stages.
- Deformation can be decreased by reducing length, width and providing ribs in the slender prismatic thin wall parts.
- The predicted simulation model is 80% accurate.

Acknowledgement

The authors are grateful to Dr. G. Sridhar, Deputy General Manager, HAL Hyderabad for his support in our study.

References

ASM Handbook, *Volume 4*: Heat Treating ASM Handbook Committee, p 841–879, 2019.

Chatelain, Jean-François and Lalonde, J.-F and Tahan, Antoine, A comparison of the distortion of machined parts resulting from residual stresses within workpieces. *International Conference on Manufacturing Engineering, Quality and Production Systems, MEQAPS – Proceedings.* 79-84, 2011.

Cheng, Weili and Finnie, Iain., Residual Stress Measurement and the Slitting Method. 10.1007/978-0-387-39030-7. , 2007.

Gao, Hanjunand Zhang, Yiduand Wu, Qiong and Liu, Chang., Influence of initial residual stress distribution on machining deformation of plate blank. *AIP Conference Proceedings*. 1829, 2017.

Garimella Sridhar and Poosa Ramesh Babu, Influence of tool parameters on machining distortion of thin wall thin floor components, *Advances in Materials and Processing Technologies,* 4:1, 61-85, 2018.

Huang, X., Sun, J. and Li, J. Finite element simulation and experimental investigation on the residual stress-related monolithic component deformation. Int J AdvManuf Technol 77, 1035–1041, 2015.

Izamshah, Raja and Y. Yuhazri, M and Hadzley, M andMd Ali, Mohd AmranandSubramonian, Sivarao, Effects of End Mill Helix Angle on Accuracy for Machining Thin-Rib Aerospace Component. *Applied Mechanics and Materials*. 315. 773-777, 2013.

Jiang, X., Li, B., Yang, J. et al. Effects of tool diameters on the residual stress and distortion induced by milling of thin-walled part. *Int J AdvManuf Technol* 68, 175–186 , 2013.

Koç, Muammerand Culp, John and Altan, Taylan., Prediction of residual stresses in quenched aluminum blocks and their reduction through cold working processes. *Journal of Materials Processing Technology* - J MATER

PROCESS TECHNOL. 174. 342-354, 2017.

Liu, Liangbaoand Sun, Jianfeiand Chen, Wuyiand Sun, Pengfei, Study on the machining distortion of aluminum alloy parts induced by forging residual stresses. *Proceedings of the Institution of Mechanical Engineers, Part B: Journal of Engineering Manufacture.*, 2015.

Masoudi, SoroushandAmini, S andSaeidi, EhsanandEslami-Chalander, Hamdollah., Effect of machining-induced residual stress on the distortion of thin-walled parts. *International Journal of Advanced Manufacturing Technology.* 10.1007/s00170-014-6281-x., 2015.

Robinson, J. S. ; Tanner, D. A. ; Truman, C. E. ; Wimpory, R. C./ Measurement and prediction of machining induced redistribution of residual stress in the aluminium alloy 7449. In: *Experimental Mechanics*., Vol. 51, No. 6. pp. 981-993b, 2011.

Schulze, V andA rrazola, Pedro andZanger, F and Osterried, J., Simulation of Distortion Due to Machining of Thin-walled Components. *Procedia CIRP*. 8., 2013.

Sridhar, Garimellaand Babu, P and Publication, IAEME., Cutting parameter optimization for minimizing machining distortion of thin wall thin floor avionic components using taguchitechnique. *International Journal of Mechanical Engineering and Technology* 0976-6359. 4. 71-78, 2013.

Tang, Z and Yu, T and Q. Xu, L and Zhanqiang, Liu., Machining deformation prediction for frame components considering multifactor coupling effects. The *International Journal of Advanced Manufacturing Technology.* 68. 10.1007/s00170- 012-4718-7, 2013.

Wei, Y., Wang, X.W. Computer simulation and experimental study of machining deflection due to original residual stress of aerospace thin-walled parts. *Int J Adv Manuf Technol* 33, 260–265, 2007. https://doi.org/10.1007/s00170-006-0470-1

Yang, Xiaweiand Zhu, JingchuanandNong, Zhishengand Lai, Zhonghongand He, Dong., FEM simulation of quenching process in A357 aluminum alloy cylindrical bars and reduction of quench residual stress through cold stretching process. *Computational Materials Science*. 69. 396–413, 2017.

Biographies

N.Vinaya Kumar is pursuing Ph.D in Mechanical Engineering in JNTU Hyderabad, India and he is active in carrying out research on optimization and simulation in distortion on slender prismatic thin wall parts.

Dr. M.Indira Rani is working as a professor, Mechanical Engineering in JNTUH College of Engineering Hyderabad, India and her research interests include Industrial Engineering, Manufacturing, Total Quality Management, Six Sigma and Entrepreneurship.